ACSNANO
www.acsnano.org
ARTICLE

Three-Dimensional Hetero-Integration of Faceted GaN on Si Pillars for Efficient Light Energy Conversion Devices

Dong Rip Kim,*[,†] Chi Hwan Lee,[‡] In Sun Cho,[§] Hanmin Jang,[†] Min Soo Jeon,[†] and Xiaolin Zheng*[,∥]

[†]School of Mechanical Engineering, Hanyang University, Seoul 133-791, South Korea
[‡]Weldon School of Biomedical Engineering, School of Mechanical Engineering, Center for Implantable Devices, and Birck Nanotechnology Center, Purdue University, West Lafayette, Indiana 47907, United States
[§]Department of Materials Science & Engineering and Energy Systems Research, Ajou University, Suwon 443-749, South Korea
[∥]Department of Mechanical Engineering, Stanford University, Stanford, California 94305, United States

Supporting Information

ABSTRACT: **An important pathway for cost-effective light energy conversion devices, such as solar cells and light emitting diodes, is to integrate III−V (*e.g.*, GaN) materials on Si substrates. Such integration first necessitates growth of high crystalline III−V materials on Si, which has been the focus of many studies. However, the integration also requires that the final III−V/Si structure has a high light energy conversion efficiency. To accomplish these twin goals, we use single-crystalline microsized Si pillars as a seed layer to first grow faceted Si structures, which are then used for the heteroepitaxial growth of faceted GaN films. These faceted GaN films on Si have high crystallinity, and their threading dislocation density is similar to that of GaN grown on sapphire. In addition, the final faceted GaN/Si structure has great light absorption and extraction characteristics, leading to improved performance for GaN-on-Si light energy conversion devices.**

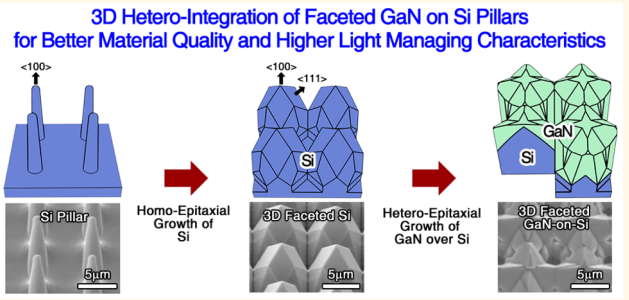

KEYWORDS: *heterointegration, 3D surface texturing, multifacet generation, GaN on Si, Optoelectronic material, silicon structure*

An important pathway for cost-effective light energy conversion devices is to heteroepitaxially grow III−V materials on Si substrates. Such integration would combine the superior optoelectronic properties of III−V materials and the well-established Si-based semiconducting technologies.[1−9] Most studies have been focusing on solving the challenge that III−V materials and Si have significant lattice and thermal mismatches. To solve the mismatch issues, many strategies have been attempted, including low-temperature nucleation,[10,11] insertion of intermediate layers between active III−V materials and Si substrates,[7,12−14] and growing III−V materials on three-dimensional (3D) Si crystal arrays at nano- and microscales.[15−19] However, in addition to heteroepitaxial growth, cost-effective light energy conversion devices will also require effective light managing structures. Here, we report the successful heteroepitaxial growth of faceted GaN crystals on tapered micron-sized Si pillars, and the resulting 3D structure exhibits excellent light managing properties. Specifically, tapered Si pillars with smooth sidewalls were first used as the epi-substrates to grow faceted Si structures. The formed faceted Si structures were then used as the substrates for the heteroepitaxial growth of faceted GaN crystals on top with high crystallinity. The resulting GaN/Si pillars form an array of inverted pyramids, which enhances both light extraction and absorption for light energy conversion devices, including light-emitting diodes and solar cells.

RESULTS AND DISCUSSION

Figure 1a schematically illustrates the basic steps to fabricate the 3D faceted Si structures, and Figure 1b shows the corresponding scanning electron microscopy (SEM) images at each step. Specifically, Si pillar arrays were first formed on top of a Si (100) wafer by photolithographic patterning and subsequent dry etching process. The Si pillars were then thoroughly cleaned by O_2 plasma and chemical cleaning processes to remove the byproduct polymers formed during the dry etching processes. The cleaned Si pillars were annealed in

Received: March 21, 2017
Accepted: May 17, 2017
Published: May 17, 2017

DOI: 10.1021/acsnano.7b01967
ACS Nano XXXX, XXX, XXX−XXX

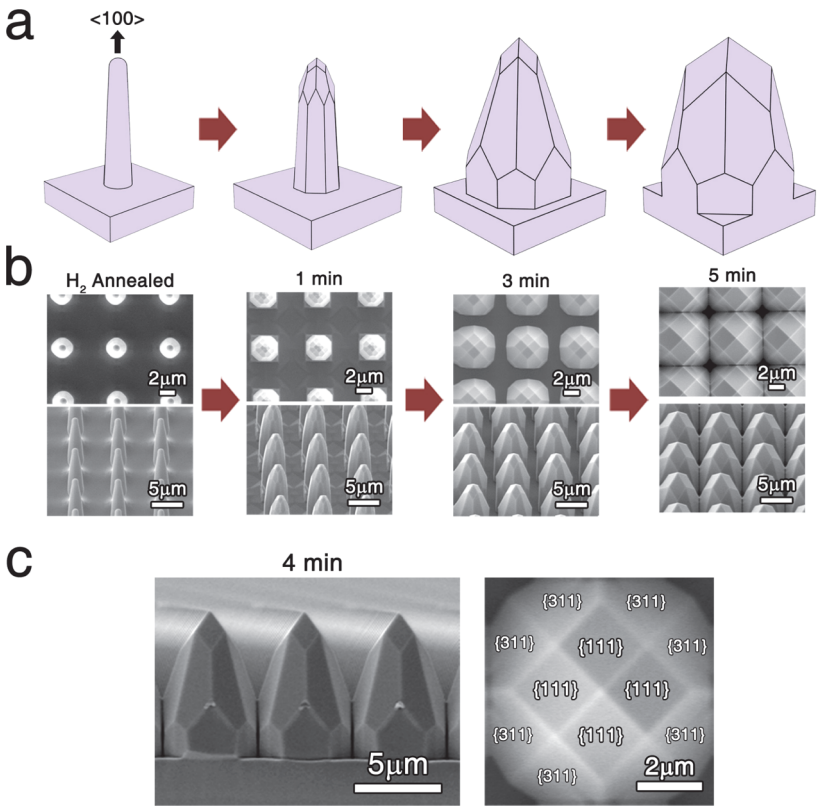

Figure 1. Fabrication and characterization of 3D faceted Si structures. (a) Schematics of the fabrication process of the 3D faceted Si structures. Si pillars were first formed using dry etching of a Si (100) wafer, followed by cleaning and annealing in H_2. Then, Si film was epitaxially grown on the Si pillars. As the epitaxial growth time increases, the morphology of the Si pillars evolves into a cone shape with faceted surfaces and a sharp tip. (b) SEM top view (upper) and tilted view (lower) images show the morphology evolution from Si pillars to 3D faceted Si structures. (c) Side view (left) and top view (right) SEM images of the representative 3D faceted Si structures (4 min growth). The four facets in the upper part of the 3D faceted Si structures were {111} crystal planes, and the eight facets in the lower part of the 3D faceted Si structures were {311}.

hydrogen for 10 min that leads to tapered Si pillars with smooth surfaces and small rounded tips, for which the crystal orientations on the sidewalls were randomized (Figure 1a and b, left). The length and tip diameter of the resulting Si pillars are about 15 and 0.8 μm, respectively. Finally, Si film was epitaxially grown on top of the smooth Si pillars. As shown in Figure 1a and b, the smooth tapered Si pillars evolve into the 3D faceted structures with sharp tips with elongated growth time (1−5 min), which is more evidenced in the enlarged views of the 3D faceted Si structures shown in Figure 1c. More detailed fabrication procedures are described in the Methods section.

To identify the crystalline structure of the 3D faceted structures on the Si (100) wafer, we performed high-resolution transmission electron microscopy (TEM) to inspect the cross-sectional samples (Figure 1c, right and Supporting Information Figure S1). The TEM analysis shows that the 3D faceted structures on the Si (100) wafer are terminated with four {111} and eight {311} crystal planes in the upper and lower parts, respectively. Similar faceted growth behaviors were also observed for vertical Si pillars fabricated on Si (110) and Si (111) wafers (Supporting Information Figures S2−S4). The dominance of those two facets is due to their slow growth rates relative to other crystallographic planes under our Si film deposition conditions.[20] Interestingly, as the growth time gets longer, the surface area of the upper four {111} facets increases, while that of the lower {311} facets decreases (Figure 1a and b). The preference of {111} over {311} facets at longer growth time is driven by the combined effects of minimizing the total surface energy and mass transport of adatoms on the 3D faceted Si structures.[21−23]

We investigate the quality of crystallinity of the 3D faceted Si structures by building a solar cell based on the 3D faceted Si structures. The as-grown 3D faceted Si structures with angled multiple facets and sharp tips naturally enhance the light absorption due to the graded refractive index effect.[24] Figure 2a compares the wavelength-dependent light absorption of 3D faceted Si structure arrays (growth time: 5 min) with and without antireflective silicon nitride coating (SiN_x, ~80 nm thick) and their corresponding planar control samples. Even without SiN_x, the 3D faceted Si structures already absorb ~92% of light in air mass 1.5 global (AM 1.5G) spectrum above the band gap of Si, which is ~1.5 times higher than the control Si planar (~62% of light absorption). The addition of SiN_x significantly increases the light absorption of Si planar to ~88%, but only slightly increases the light absorption of the 3D faceted Si to ~95%. The 3D faceted Si structures also exhibit less angle-dependent light absorption according to the finite-difference time-domain (FDTD) simulations as shown in Figure 2b. The 3D faceted Si structures with/without SiN_x exhibit little angle-dependent light absorption, while the light absorption of Si planar samples drops quickly as the light incident angle approaches to 80°. The less angle dependency for the 3D faceted Si structure light absorption was attributed

DOI: 10.1021/acsnano.7b01967
ACS Nano XXXX, XXX, XXX−XXX

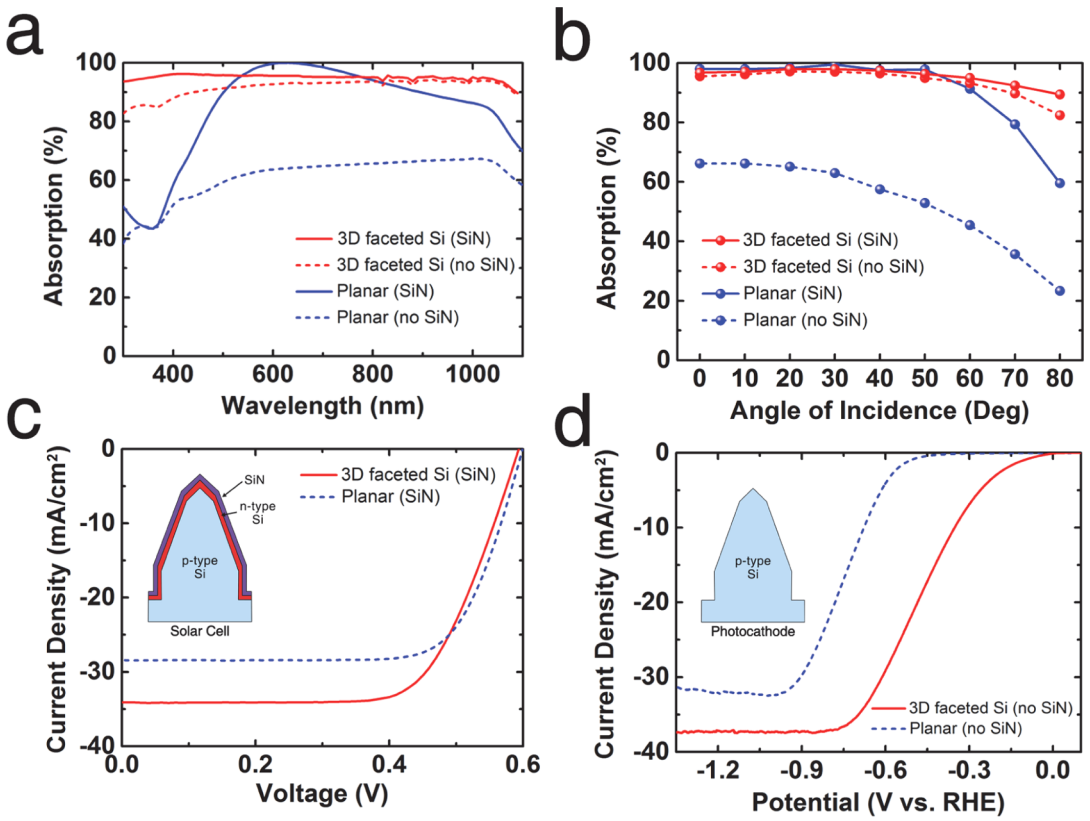

Figure 2. Comparison of the performance of 3D faceted Si structures *versus* Si planar solar cells and photocathodes for HER. (a) Wavelength-dependent light absorption of 3D faceted Si structures (red) and planar Si (blue) with/without SiN_x antireflective layer. (b) Integrated light absorption dependence on incidence angle for 3D faceted Si structures (red) and planar Si (blue) with/without SiN_x antireflective layer. (c) The photovoltaic properties of 3D faceted Si (red) and planar Si (blue) solar cells. Both have a 80 nm-thick SiN_x on their tops. (d) The PEC properties of 3D faceted Si (red) and planar Si (blue) photocathodes for HER. Both have no antireflective layer on their top surfaces.

to their angled multiple facets, which causes the refractive index profile to be less sensitive to the incident light angle. The less angle-dependent light absorption properties can be exploited to deploy the solar cells without a solar tracker. Figure 2c shows the representative light current density *versus* voltage curves under AM 1.5G illumination. We tested five 3D faceted Si structure solar cells and five control planar solar cells, respectively. Statistically, the 3D faceted Si structure solar cell has an efficiency (η) = 13.7 ± 0.2%, open circuit voltages (V_{oc}) = 0.591 ± 0.006 V, short circuit current densities (J_{sc}) = 33.9 ± 0.2 mA/cm^2, and fill factor (FF) = 0.687 ± 0.010, and they are better than the control planar solar cell (η = 12.3 ± 0.3%, V_{oc} = 0.601 ± 0.004 V, J_{sc} = 28.2 ± 0.1 mA/cm^2, FF = 0.724 ± 0.013). It should be noted that the V_{oc} values are comparable between 3D structures and planar cases even though the former has about three times higher surface area, which suggests that the 3D faceted structures are of high crystallinity. The comparable V_{oc} in the 3D solar cells is attributed to the combined effects of high crystallinity of 3D faceted Si, its higher light absorption (~1.1 times), and good front surface passivation by silicon nitride deposited by PECVD. Moreover, the 1.2 times higher J_{sc} of the 3D faceted structures comes from the ~1.1 times higher light absorption than the control planar and the better charge-carrier collection in longer wavelength region. The efficiency of our 3D faceted Si structure solar cells can be further improved by device optimizations, such as front and bottom surface passivation, and design of the electrode configuration.

To investigate the surface properties of the 3D faceted Si structures, we further fabricate Si photocathodes in photoelectrochemical (PEC) water splitting cells. The detailed fabrication procedures for the Si photocathodes are described in the Methods section. Figure 2d shows a representative photocurrent density *versus* applied potential (J–V) curve of a p-type 3D faceted Si photocathode in an electrolyte of 0.5 M H_2SO_4 under AM 1.5G illumination with comparison to a control Si (100) planar photocathode. The saturation photocurrent of the 3D faceted Si photocathode reaches 37 mA/cm^2, which is ~1.2 times higher than that of the control Si planar (31 mA/cm^2). The enhancement is due to the higher light absorption (the integrated light absorption of 95%) by the 3D faceted Si structures in aqueous environment than that of the planar Si (the integrated light absorption of 74%) (Supporting Information Figure S5). More interestingly, the onset potential for the 3D faceted Si photocathode is about −0.02 V *versus* reversible hydrogen electrode (RHE), which is about 430 mV more anodic than the onset potential of a planar Si (Figure 2d). We believe that the large 430 mV anodic shift is caused by the increase of surface area,[25] but more importantly by the exposure of the relatively high index facets,[26,27] such as {311} crystal planes, which shows that the kinetics of hydrogen evolution reaction (HER) on Si can be accelerated by exposing specific facets.

We demonstrate that the 3D faceted Si structures can be used as effective seeds for the heteroepitaxial growth of 3D faceted GaN crystals on top (Figure 3). Here, we used metal organic chemical vapor deposition (MOCVD) to grow GaN

DOI: 10.1021/acsnano.7b01967
ACS Nano XXXX, XXX, XXX−XXX

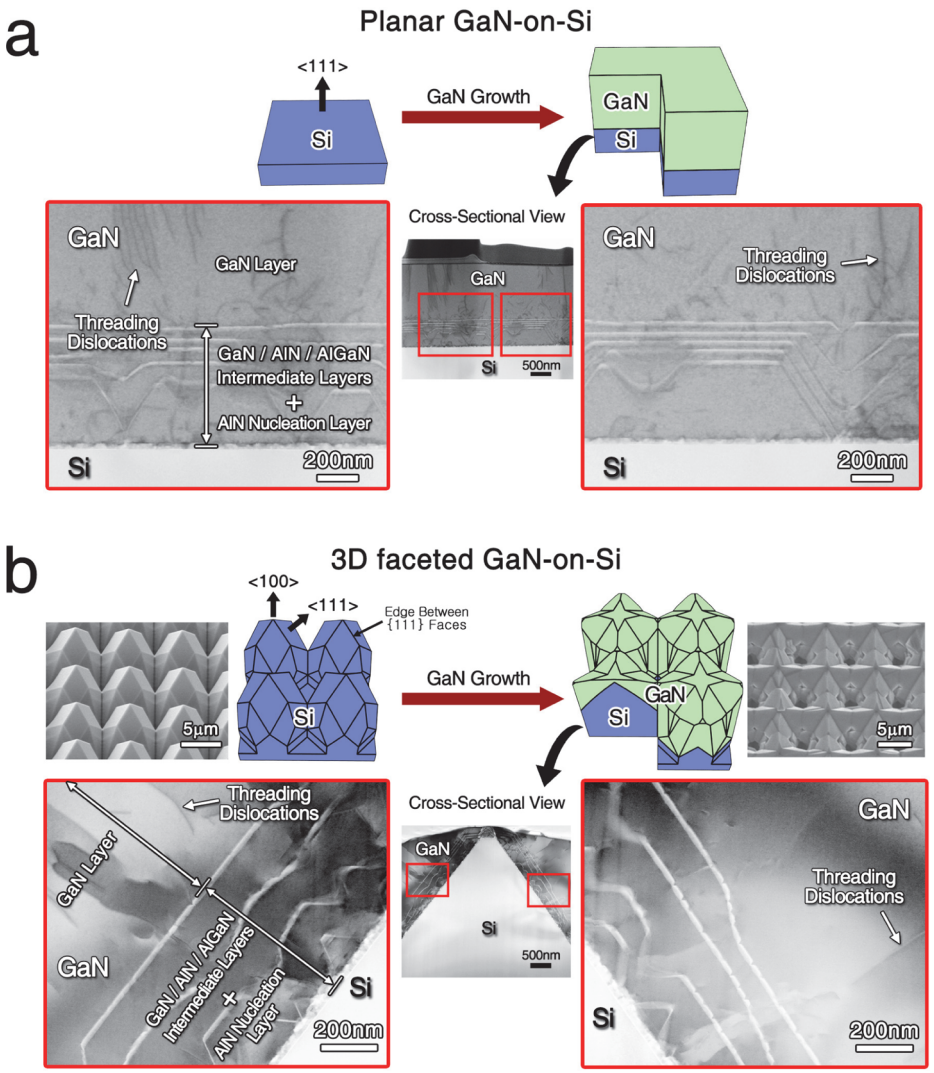

Figure 3. SEM and TEM images of heteroepitaxial growth of GaN on (a) planar Si and (b) 3D faceted Si. The black lines in the GaN layer are indications of dislocation. The dislocation density of GaN is less in the 3D faceted Si structures than that in planar Si. The deposited films on Si include the AlN nucleation layer, the GaN/AlN/AlGaN intermediate layers, and the GaN layer. The white lines near the surface indicate the AlGaN layers in the GaN/AlN/AlGaN intermediate layers. Heteroepitaxial growth of GaN on 3D faceted Si structures not only forms continuous GaN layer but also constructs an inverted pyramid shape.

over both 3D faceted Si structures (with four {111} crystal planes in the upper part) and control Si (111) planar wafers (see Methods section for details). The Si (111) planar wafers are studied as a control sample to illustrate the benefits of 3D faceted Si structures. For both cases, to improve the quality of the deposited 1 μm-thick GaN on Si, AlN was first deposited on Si as a nucleation layer, followed by the deposition of GaN/AlN/AlGaN intermediate layers. The total thickness of AlN nucleation layer and GaN/AlN/AlGaN intermediate layers was around 600 nm. Figure 3a and b shows the SEM and TEM images of the MOCVD deposited GaN film on a Si (111) planar wafer and 3D faceted Si structures (Figure 1b, 5 min). The quality of GaN is evaluated based on the threading dislocation density (TDD), which is estimated here by measuring the total length of all TDD in the cross-sectional TEM images (Figure 3) and dividing the total length by the crystal volume. The TDD for the GaN layer on 3D faceted Si structures was measured to be around 3.4×10^8 cm^{-2}, which is about three times lower than that of the control GaN-on-Si planar sample (11.3×10^8 cm^{-2}). The smaller TDD of GaN on the 3D faceted Si structures is attributed to the fact that the sharp edges between the {111} faceted surfaces of 3D faceted Si structures help to release the stresses in the deposited GaN film resulting from a large lattice constant and thermal expansion coefficient mismatches.[3] Significantly, the TDD of GaN on 3D faceted Si structures is comparable with that of the conventional GaN deposited over the sapphire substrate ($3.6-6.4 \times 10^8$ cm^{-2}),[28] which shows the great promise of using 3D faceted Si structures as substrates for heteroepitaxial growth of high-quality GaN on top for LED applications.

Heteroepitaxial growth of GaN on the 3D faceted Si structures not only results in continuous GaN films with higher quality but also creates highly faceted 3D GaN crystals, as shown in Figures 3b and 4a. This morphology of GaN is formed because the growth of GaN is more favorable on the Si {111} crystal planes than others due to their three-fold surface symmetry,[3,29] but the growth is spatially confined due to the proximity of the neighboring GaN crystals (Figure 4a). Specifically, the favorable GaN growth on Si {111} crystal planes results in the thicker layer of GaN on the {111} crystal

DOI: 10.1021/acsnano.7b01967
ACS Nano XXXX, XXX, XXX−XXX

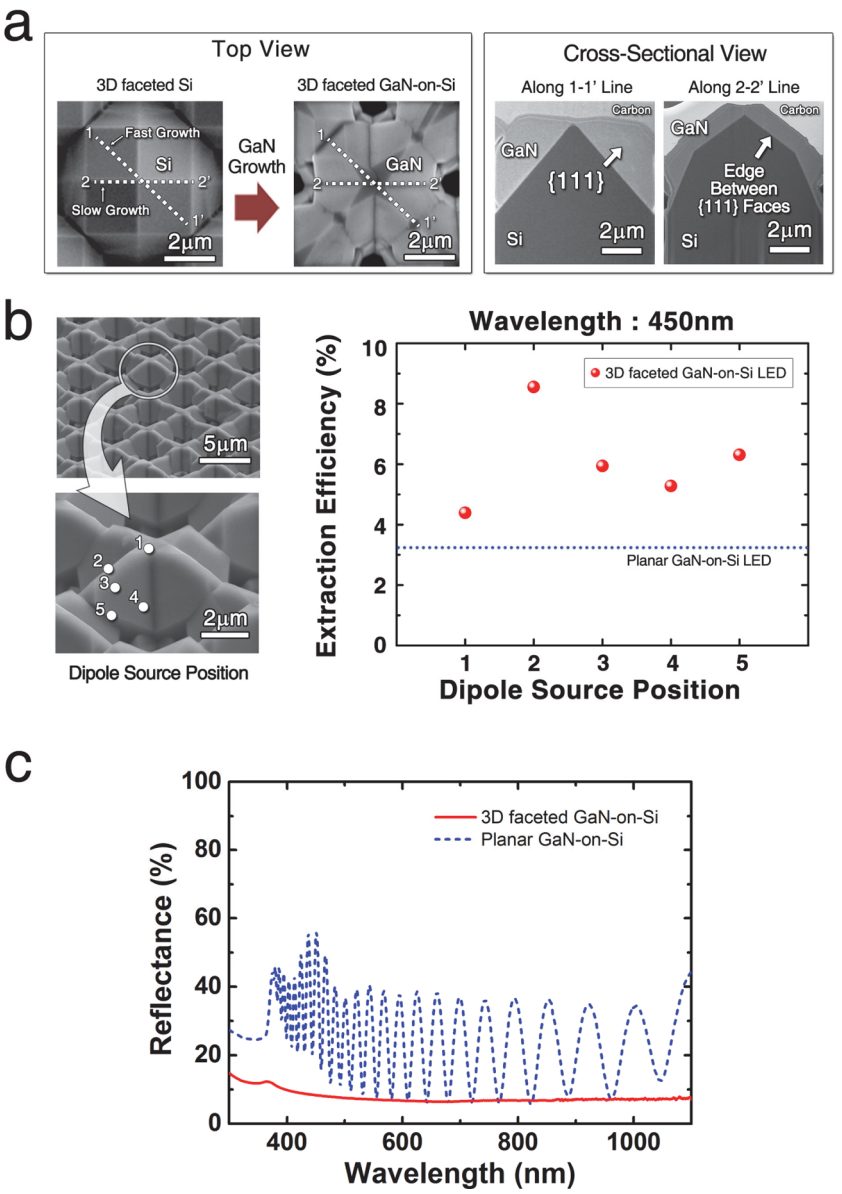

Figure 4. Formation of 3D GaN crystals on the 3D faceted Si structures and their light managing properties. (a) Morphology evolution as GaN is grown on the 3D faceted Si structures. (Left) SEM top views of the 3D faceted Si structures and the 3D faceted GaN-on-Si structures. (Right) SEM cross-sectional views of the 3D faceted GaN-on-Si structures along 1−1′ and 2−2′ lines in the left, respectively. More favorable growth of GaN layer on the Si {111} crystal plane (see SEM cross-sectional view along 1−1′ line) results in the morphology evolution, combined with the limitation by the proximity of the next GaN crystals. (b) Simulated light extraction efficiency of the 3D faceted GaN-on-Si LEDs, compared to the GaN-on-Si planar LEDs, as a function of dipole source positions. (c) Wavelength-dependent light reflection of 3D faceted GaN-on-Si structures (red) and planar GaN-on-Si (blue).

planes of the 3D faceted Si structures (the cross-sectional view along 1−1′ line in Figure 4a) and the relatively thinner layer of GaN on the edge between the {111} crystal planes (the cross-sectional view along 2−2′ line in Figure 4a). When combined with the proximity of the neighboring GaN crystals, this difference of GaN growth rate on Si leads to the morphology evolution to the inverted pyramids from cone shapes. To evaluate the potential of those faceted GaN crystals on Si for LEDs, we calculated their light extraction efficiencies using the FDTD simulations and compared those with the control planar GaN/Si for the wavelength of 450 nm in terms of specific dipole source locations. As shown in Figure 4b, the light extraction efficiency for 3D faceted GaN-on-Si outperforms that of the planar over all the locations. In addition, if the 3D faceted GaN-on-Si is utilized for LED, we expect that the 3D faceted GaN-on-Si can have better external quantum efficiency and electroluminescence intensity than the planar due to the higher quality of GaN and can exhibit tunable colors in the visible range due to the change of the equipotential plane shapes along the 3D structure of GaN resulting from the change of the electric field.[30] Finally, we investigate the structural merit of 3D faceted GaN-on-Si structures to enhance the light absorption. Figure 4c shows the measurement results of wavelength-dependent light reflection of 3D faceted GaN-on-Si and control planar. The 3D faceted GaN-on-Si structures significantly reduce the reflection of light to ∼7% in AM 1.5G spectrum above the band gap of Si, while the control GaN-on-

DOI: 10.1021/acsnano.7b01967
ACS Nano XXXX, XXX, XXX−XXX

Si planar reflects ~26% of the light. This indicates the potential of our method to realize effective light-harvesting devices.

CONCLUSIONS

In summary, we demonstrated that tapered micrometer-sized Si pillars with smooth sidewalls are effective seed substrates for homoepitaxial growth of 3D faceted Si structures with predominantly exposed {111} and {311} crystal planes. These 3D faceted Si structures, when used for solar cells and solar hydrogen production cells, greatly improve the light energy conversion performances due to their tapered shapes and high crystallinity. These 3D faceted Si structures are excellent seeds for the heteroepitaxial growth of high-quality GaN since the sharp edges of 3D faceted Si structures help to release stresses, which may facilitate the use of Si substrates for GaN-based LEDs and solar cells. Our methodology of creating highly faceted crystal arrays can be applied to other optoelectronic materials to improve their device performance.

METHODS

Fabrication of the 3D Faceted Si Structures. The single-crystalline p-type Si (100) wafer (a thickness of 500 μm, a resistivity of 0.1−0.9 Ω·cm) was patterned using photolithography and dry-etched to form Si pillar arrays (3 μm diameter and 15 μm length). The diameters of the Si pillars were further reduced to 0.8−0.9 μm by using isotropic dry etch (a plasma power of 600W, and a gas of only SF_6 with 130 sccm). The Si pillars were thoroughly cleaned by O_2 plasma, followed by the wet chemical cleaning process. The Si pillars were thermally annealed at 1050 °C and 40 Torr in a H_2 environment for 10 min. The p-type Si was grown over the Si pillars at 1050 °C and 60 Torr with 370 sccm dichrolosilane (DCS), 110 sccm p-type dopant gas (a mixing ratio of 20% of B_2H_6 (1% diluted in H_2) and 80% of H_2), 110 sccm HCl, and 20 slm H_2 gases for 5 min. The measured resistivity of the epitaxially grown p-type Si was about 0.1 Ω·cm.

Fabrication of the 3D Faceted Si Solar Cells and Photocathodes. The 3D faceted Si solar cells were fabricated by forming a p−n junction using n-type dopant diffusion at 950 °C for 1 min 25 s, flowing N_2 gas through a $POCl_3$ bubbler. The resistivity of the n-type Si film was about 0.001 Ω·cm. An 80 nm-thick SiN_x antireflective layer was deposited on top of the n-type Si at 350 °C using plasma-enhanced chemical vapor deposition (PECVD). The n-type Si contact was metallized with Ti/Pd/Ag (thicknesses of 5/300/700 nm), and the p-type Si contact was metallized with Al (a thickness of 700 nm). The 3D faceted Si photocathodes were realized by metallizing the bottom side of the p-type 3D faceted Si structures with a 700 nm-thick Al film. The control Si planar solar cells and photocathodes were fabricated over Si (100) wafers with the identical processes.

Fabrication of the 3D Faceted GaN-on-Si. The epitaxial growth of GaN over the 3D faceted Si structures was carried out using MOCVD with precursors of trimethylgallium (TMGa), trimethylaluminum (TMAl), and ammonia (NH_3) for Ga, Al, and N and with carrier gas of H_2. To improve the quality of GaN deposition on Si, GaN/AlN/AlGaN intermediate layers were introduced after the AlN nucleation layer was deposited onto the surface of the 3D faceted Si structures. The target thickness of AlN nucleation layer and GaN/AlN/AlGaN intermediate layers was ~600 nm. First, the AlN nucleation layer was formed by depositing a 20 nm-thick AlN layer at 1060 °C (pressure of 60 Torr and flow rates of 35 sccm TMAl and 2200 sccm NH_3), followed by growing 30 nm-thick AlN layer at 1350 °C (pressure of 60 Torr and flow rates of 35 sccm TMAl and 500 sccm NH_3). Second, five GaN/AlN/AlGaN intermediate layers were deposited over the AlN nucleation layers. One GaN/AlN/AlGaN intermediate layer includes 60 nm-thick GaN layer (flow rates of 36 sccm TMGa and 2200 sccm NH_3), 10 nm-thick AlN layer (flow rates of 35 sccm TMAl and 6000 sccm NH_3), and 40 nm-thick AlGaN layer (flow rates of 30 sccm TMAl, 36 sccm TMGa, and 2200 sccm NH_3). All the intermediate layers were deposited at 1060 °C and at 60 Torr. Finally, 1 μm-thick undoped GaN layer was grown over the GaN/AlN/AlGaN intermediate layer at 1060 °C and at 60 Torr (flow rates of 36 sccm TMGa and 8000 sccm NH_3). The layer thickness described here is estimated from the thin-film growth rate. Importantly, the fabrication conditions of the control GaN-on-Si planar samples were identical to those of the 3D faceted GaN-on-Si structures, and they were fabricated at the same time.

Characterizations. For optical properties, the light reflection was measured by a photodetector in an integrating sphere using a xenon lamp coupled to a monochromator (Model QEX7, PV Measurement). The light absorption was calculated by subtracting the reflection (%) from 100 (%). The solar cell properties were characterized using a semiconductor analyzer (Model 4200-SCS, Keithley) under AM 1.5G illumination (Class AAA solar simulator, Model 94063A, Oriel) after careful calibration with a reference cell and a readout meter for solar simulator irradiation (Model 91150 V, Newport). The area of solar cells was 1 cm^2. The PEC measurements for HER were conducted in an electrolyte of 0.5 M H_2SO_4 (pH ~ 0) using a potentiostat (Model SP200, Bio-Logic) with three electrodes: Si as the working electrode (an illuminated area of 0.502 cm^2), a Pt wire (a surface area of 0.8 mm^2) as the counter electrode, and Ag/AgCl as the reference electrode, under AM 1.5G illumination (Class AAA solar simulator, Model 94063A, Oriel, 100 mW/cm^2). Before measurements, the native Si oxides were removed by soaking in 16% HF solution for 30 s, and then the Si surfaces were stabilized in the electrolyte by applying −1.5 V with respect to the Ag/AgCl reference electrode for 5 min.

FDTD Simulations. Optical simulations were carried out using a commercial FDTD software (Lumerical Solutions, Inc.). For the light absorption dependency on the incidence angle, the calculations were performed in a single unit cell of 3D structures with bloch boundary conditions in the x and y directions and with perfectly matched layer boundary conditions in the z direction. A planewave source in the wavelength ranging from 400 to 1100 nm was incident at an angle with respect to the z direction. The refractive index of SiN_x was set as 1.96. The refractive index of GaN was set as 2.49. For calculation of the light extraction efficiency in the GaN-on-Si LEDs, the 3D faceted GaN-on-Si structure was divided into eight parts from the top view, and each of the eight parts was set as a single unit cell. Dipole source mimicking quantum wells as light source was located at 300 nm below the GaN surface in the single unit cell, and the light intensity was measured from the top side. The extraction efficiency was calculated by dividing the light intensity with the power of dipole source.

ASSOCIATED CONTENT

Supporting Information

The Supporting Information is available free of charge on the ACS Publications website at DOI: 10.1021/acsnano.7b01967.

SEM and TEM image of 3D faceted Si structures formed on a Si (100) wafer, morphology change upon the epitaxial growth of Si over Si pillars fabricated on Si (100), Si (110), and Si (111) wafers, SEM and TEM images of 3D faceted Si structures formed on a Si (110) wafer, SEM and TEM image of 3D faceted Si structures formed on a Si (111) wafer, light absorption curves of 3D faceted Si structures and planar Si in water and air (PDF)

AUTHOR INFORMATION

Corresponding Authors

*E-mail: dongrip@hanyang.ac.kr.
*E-mail: xlzheng@stanford.edu.

ORCID

Dong Rip Kim: 0000-0001-6398-9483
In Sun Cho: 0000-0001-5622-7712
Hanmin Jang: 0000-0002-7724-4244

DOI: 10.1021/acsnano.7b01967
ACS Nano XXXX, XXX, XXX−XXX

Author Contributions

D.R.K. and X.L.Z. designed the experiments. D.R.K., C.H.L., I.S.C., H.J., M.S.J., and X.L.Z. performed experiments and analyzed the data. D.R.K. and X.L.Z. prepared the manuscript.

Notes

The authors declare no competing financial interest.

ACKNOWLEDGMENTS

This research is supported by Basic Science Research Program (NRF-2015R1C1A1A02037752) and International Research and Development Program (NRF-2016K1A3A1A32913073) through the National Research Foundation of Korea (NRF) funded by the Ministry of Science, ICT, and Future Planning of Korea. This work is also supported by the Intelligent Synthetic Biology Center of Global Frontier Project funded by the Ministry of Science, ICT, and Future Planning of Korea (NRF-2012M3A6A8054889).

REFERENCES

(1) Falub, C. V.; von Kanel, H.; Isa, F.; Bergamaschini, R.; Marzegalli, A.; Chrastina, D.; Isella, G.; Muller, E.; Niedermann, P.; Miglio, L. Scaling Hetero-Epitaxy From Layers to Three-Dimensional Crystals. *Science* **2012**, *335*, 1330−1334.

(2) Justice, J.; Bower, C.; Meitl, M.; Mooney, M. B.; Gubbins, M. A.; Corbett, B. Wafer-Scale Integration of Group III-V Lasers on Silicon Using Transfer Printing of Epitaxial Layers. *Nat. Photonics* **2012**, *6*, 610−614.

(3) Zhu, D.; Wallis, D. J.; Humphreys, C. J. Prospects of III-Nitride Optoelectronics Grown on Si. *Rep. Prog. Phys.* **2013**, *76*, 106501.

(4) Luo, Z.; Jiang, Y.; Myers, B. D.; Isheim, D.; Wu, J.; Zimmerman, J. F.; Wang, Z.; Li, Q.; Wang, Y.; Chen, X.; Dravid, V. P.; Seidman, D. N.; Tian, B. Atomic Gold−Enabled Three-Dimensional Lithography for Silicon Mesostructures. *Science* **2015**, *348*, 1451−1455.

(5) Jiang, Y.; Carvalho-de-Souza, J. L.; Wong, R. C. S.; Luo, Z.; Isheim, D.; Zuo, X.; Nicholls, A. W.; Jung, I. W.; Yue, J.; Liu, D.-J.; Wang, Y.; De Andrade, V.; Xiao, X.; Navrazhnykh, L.; Weiss, D. E.; Wu, X.; Seidman, D. N.; Bezanilla, F.; Tian, B. Heterogeneous Silicon Mesostructures for Lipid-Supported Bioelectric Interfaces. *Nat. Mater.* **2016**, *15*, 1023−1030.

(6) Day, R. W.; Mankin, M. N.; Gao, R.; No, Y.-S.; Kim, S.-K.; Bell, D. C.; Park, H.-G.; Lieber, C. M. Plateau−Rayleigh Crystal Growth of Periodic Shells on One-Dimensional Substrates. *Nat. Nanotechnol.* **2015**, *10*, 345−352.

(7) Hus, J.-W.; Chen, C.-C.; Lee, M.-J.; Liu, H.-H.; Chyi, J.-I.; Huang, M. R. S.; Liu, C.-P.; Wei, T.-C.; He, J.-H.; Lai, K.-Y. Bottom-Up Nano-Heteroepitaxy of Wafer-Scale Semipolar GaN on (001) Si. *Adv. Mater.* **2015**, *27*, 4845−4850.

(8) Chen, S.; Li, W.; Wu, J.; Jiang, Q.; Tang, M.; Shutts, S.; Elliott, S. N.; Sobiesierski, A.; Seeds, A. J.; Ross, I.; Smowton, P. M.; Liu, H. Electrically Pumped Continuous-Wave III−V Quantum Dot Lasers on Silicon. *Nat. Photonics* **2016**, *10*, 307−311.

(9) Yao, M.; Sheng, C.; Ge, M.; Chi, C.-Y.; Cong, S.; Nakano, A.; Dapkus, P. D.; Zhou, C. Facile Five-Step Heteroepitaxial Growth of GaAs Nanowires on Silicon Substrates and the Twin Formation Mechanism. *ACS Nano* **2016**, *10*, 2424−2435.

(10) Ishikawa, H.; Yamamoto, K.; Egawa, T.; Soga, T.; Jimbo, T.; Umeno, M. Thermal Stability of GaN on (1 1 1) Si Substrate. *J. Cryst. Growth* **1998**, *189*−*190*, 178−182.

(11) Takemoto, K.; Murakami, H.; Iwamoto, T.; Matsuo, Y.; Kangawa, Y.; Kumagai, Y.; Koukitu, A. Growth of GaN Directly on Si(111) Substrate by Controlling Atomic Configuration of Si Surface by Metalorganic Vapor Phase Epitaxy. *Jpn. J. Appl. Phys.* **2006**, *45*, L478.

(12) Krost, A.; Dadgar, A. GaN-Based Devices on Si. *Phys. Status Solidi A* **2002**, *194*, 361−375.

(13) Dadgar, A.; Poschenrieder, M.; Bläsing, J.; Fehse, K.; Diez, A.; Krost, A. Thick, Crack-Free Blue Light-Emitting Diodes on Si(111) Using Low-Temperature AlN Interlayers and *in situ* Si_xN_y Masking. *Appl. Phys. Lett.* **2002**, *80*, 3670−3672.

(14) Alaskar, Y.; Arafin, S.; Wickramaratne, D.; Zurbuchen, M. A.; He, L.; McKay, J.; Lin, Q.; Goorsky, M. S.; Lake, R. K.; Wang, K. L. Towards Van Der Waals Epitaxial Growth of GaAs on Si Using a Graphene Buffer Layer. *Adv. Funct. Mater.* **2014**, *24*, 6629−6638.

(15) Sawaki, N.; Hikosaka, T.; Koide, N.; Tanaka, S.; Honda, Y.; Yamaguchi, M. Growth and Properties of Semi-Polar GaN on a Patterned Silicon Substrate. *J. Cryst. Growth* **2009**, *311*, 2867−2874.

(16) Jiang, X.; Tian, B.; Xiang, J.; Qian, F.; Zheng, G.; Wang, H.; Mai, L.; Lieber, C. M. Rational Growth of Branched Nanowire Heterostructures with Synthetically Encoded Properties and Function. *Proc. Natl. Acad. Sci. U. S. A.* **2011**, *108*, 12212−12216.

(17) Hocevar, M.; Immink, G.; Verheijen, M.; Akopian, N.; Zwiller, V.; Kouwenhoven, L.; Bakkers, E. Growth and Optical Properties of Axial Hybrid III−V/Silicon Nanowires. *Nat. Commun.* **2012**, *3*, 1266.

(18) Stark, C. J. M.; Detchprohm, T.; Lee, S. C.; Jiang, Y.-B.; Brueck, S. R. J.; Wetzel, C. Green Cubic GaInN/GaN Light-Emitting Diode on Microstructured Silicon (100). *Appl. Phys. Lett.* **2013**, *103*, 232107.

(19) Bayram, C.; Ott, J. A.; Shiu, K.-T.; Cheng, C.-W.; Zhu, Y.; Kim, J.; Razeghi, M.; Sadana, D. K. Cubic Phase GaN on Nano-Grooved Si (100) *via* Maskless Selective Area Epitaxy. *Adv. Funct. Mater.* **2014**, *24*, 4492−4496.

(20) Hirayama, H.; Hiroi, M.; Ide, T. {311} Facets of Selectively Grown Epitaxial Si Layers on SiO_2-Patterned Si(100) Surfaces. *Phys. Rev. B: Condens. Matter Mater. Phys.* **1993**, *48*, 17331.

(21) Aoyama, T.; Ikarashi, T.; Miyanaga, K.; Tatsumi, T. Facet Formation Mechanism of Silicon Selective Epitaxial Layer by Si Ultrahigh Vacuum Chemical Vapor Deposition. *J. Cryst. Growth* **1994**, *136*, 349−354.

(22) Li, S.; Xiang, Q.; Wang, D.; Wang, K. L. Modeling of Facet Growth on Patterned Si Substrate in Gas Source MBE. *J. Cryst. Growth* **1995**, *157*, 185−189.

(23) Lim, S.-H.; Song, S.; Lee, G.-D.; Yoon, E.; Lee, J.-H. Facet Evolution in Selective Epitaxial Growth of Si by Cold-Wall Ultrahigh Vacuum Chemical Vapor Deposition. *J. Vac. Sci. Technol., B: Nanotechnol. Microelectron.: Mater., Process., Meas., Phenom.* **2004**, *22*, 682.

(24) Zhu, J.; Yu, Z.; Burkhard, G. F.; Hsu, C.-M.; Connor, S. T.; Xu, Y.; Wang, Q.; McGehee, M.; Fan, S.; Cui, Y. Optical Absorption Enhancement in Amorphous Silicon Nanowire and Nanocone Arrays. *Nano Lett.* **2009**, *9*, 279−282.

(25) Oh, J.; Deutsch, T. G.; Yuan, H.-C.; Branz, H. M. Nanoporous Black Silicon Photocathode for H_2 Production by Photoelectrochemical Water Splitting. *Energy Environ. Sci.* **2011**, *4*, 1690−1694.

(26) Tian, N.; Zhou, Z.-Y.; Sun, S.-G.; Ding, Y.; Wang, Z. L. Synthesis of Tetrahexahedral Platinum Nanocrystals with High-Index Facets and High Electro-Oxidation Activity. *Science* **2007**, *316*, 732−735.

(27) Leng, M.; Liu, M.; Zhang, Y.; Wang, Z.; Yu, C.; Yang, X.; Zhang, H.; Wang, C. Polyhedral 50-Facet Cu_2O Microcrystals Partially Enclosed by {311} High-Index Planes: Synthesis and Enhanced Catalytic CO Oxidation Activity. *J. Am. Chem. Soc.* **2010**, *132*, 17084−17087.

(28) Li, Y.; You, S.; Zhu, M.; Zhao, L.; Hou, W.; Detchprohm, T.; Taniguchi, Y.; Tamura, N.; Tanaka, S.; Wetzel, C. Defect-Reduced Green GaInN/GaN Light-Emitting Diode on Nanopatterned Sapphire. *Appl. Phys. Lett.* **2011**, *98*, 151102.

(29) Lee, J.; Tak, Y.; Kim, J.-Y.; Hong, H.-G.; Chae, S.; Min, B.; Jeong, H.; Yoo, J.; Kim, J.-R.; Park, Y. Growth of High-Quality InGaN/GaN LED Structures on (111) Si Substrates with Internal Quantum Efficiency Exceeding 50%. *J. Cryst. Growth* **2011**, *315*, 263−266.

(30) Hong, Y. J.; Lee, C. H.; Yoon, A.; Kim, M.; Seong, H. K.; Chung, H. J.; Sone, C.; Park, Y. J.; Yi, G. C. Visible-Color-Tunable Light-Emitting Diodes. *Adv. Mater.* **2011**, *23*, 3284−3288.

DOI: 10.1021/acsnano.7b01967
ACS Nano XXXX, XXX, XXX−XXX